NANO · MICRO small
www.small-journal.com

Selective Toluene Oxidation Using Sulfur-Doped Polymeric Carbon Nitride Photocatalysts

Bayan Abed, Venugopala Rao Battula, Michael Volokh, Devesh Garg, Tirza Shmila, Gabriel Mark, Ayelet Tashakory, Alexander I. Shames, and Menny Shalom**

Selective traditional oxidation of toluene to high-value products like benzyl alcohol, benzaldehyde, and benzoic acid faces significant challenges due to high dissociation energy requirements, harsh reaction conditions, and complex product distributions. While photocatalysis using O_2 as an oxidant offers a green alternative, developing efficient and durable photocatalysts for selective oxidation in both batch and flow systems remains challenging. Here, sulfur-doped polymeric carbon nitride (S-CN) is demonstrated as a versatile photocatalyst for selective toluene oxidation, applicable in both powder form and as binder-free panels across various reactor configurations and solvents. Tuning S monomer content within supramolecular assemblies that serve as S-CN precursors, allows enhanced light absorption, optimized band positions, high specific surface area, and tailored structural properties of the ensuing catalysts. The optimized photocatalyst achieves high product selectivity, yielding ~72% benzaldehyde and ~26% benzoic acid after 24 h. Mechanistic studies confirm the concurrent oxidation and reduction reactions occurring and the roles of $O_2^{\cdot-}$ and $^1O_2$. Extended reaction time (48 h) enables selective benzoic acid production (73.4%) with minimal benzaldehyde formation (<1%), demonstrating excellent product control.

1. Introduction

C(sp^3)−H bond oxidation to realize cost-effective conversion of toluene to value-added products—such as benzyl alcohol, benzaldehyde, and benzoic acid—is highly appealing but still remains a major industrial challenge due to its high dissociation energy (412 kJ mol^{-1}) and operational requirements (high temperature and pressure), which lead to multiple oxidation products.[1,2] Particularly, selective oxidation to benzaldehyde holds enormous significance due to its essential use in the making of perfumes, pharmaceuticals, dyes, plasticizers, and other valuable chemicals.[3,4] Benzoic acid—another possible oxidation product—finds its use in topical medications, dyes, fragrances, and insect repellents.[5]

Traditionally, benzaldehyde is prepared by the $-CH_3$ chlorination of toluene, followed by hydrolysis in the presence of a base.[6] This multi-step process requires harsh reaction conditions and releases chlorinated impurities. The available alternative routes for direct toluene oxidation in the vapor/liquid phase demand harsh reaction conditions and suffer from low selectivity due to favorable deep oxidation.[7–13] Therefore, benign, selective toluene oxidation to benzaldehyde and benzoic acid is of great importance.

Photocatalytic toluene oxidation, using O_2 as a green oxidant, offers simplicity due to mild reaction conditions and good selectivity to the desired oxidation product. Over the years, many heterogeneous photocatalysts—including metal oxides,[3,14–19] metal sulfides,[20,21] perovskites,[1,22] polymeric carbon nitride (CNs) or their composites,[23–29] and covalent triazine frameworks or other organic frameworks[30–33]—have been utilized to achieve efficient toluene oxidation to benzaldehyde. However, despite these encouraging results, photocatalytic toluene oxidation is still far from having practical applications. Thus, the design of efficient, scalable, selective, low-cost, and stable photocatalysts for toluene oxidation, as powders (continuously stirred photocatalysis) or as photocatalytic panels for batch and flow reactor configurations, remains a challenge.

CNs have emerged as promising heterogeneous photocatalysts due to their ease of synthesis, tunable photophysical properties, and stability.[34–37] Notably, their appropriate valance band (VB) can facilitate mild oxidation of C(sp^3)−H bond of toluene, while the conduction band (CB) position enables an effective molecular oxygen (O_2) reduction to a superoxide radical ($O_2^{\cdot-}$), a major reactive oxygen species involved in the toluene oxidation

B. Abed, V. R. Battula, M. Volokh, D. Garg, T. Shmila, G. Mark, A. Tashakory, M. Shalom
Department of Chemistry and Ilse Katz Institute for Nanoscale Science and Technology
Ben-Gurion University of the Negev
Beer-Sheva 8410501, Israel
E-mail: battula@bgu.ac.il; mennysh@bgu.ac.il
A. I. Shames
Department of Physics
Ben-Gurion University of the Negev
Beer-Sheva 8410501, Israel

The ORCID identification number(s) for the author(s) of this article can be found under https://doi.org/10.1002/smll.202501230

DOI: 10.1002/smll.202501230

mechanism.[23] Thus, CN-based photocatalysts can be an excellent choice for performing toluene oxidation to benzaldehyde. However, despite progress in the synthesis of CN and their photocatalytic activity for toluene oxidation,[23] their performance is still limited by low specific surface area, charge recombination, and non-optimal visible-light absorption.[23,38]

Herein, we demonstrate a facile synthesis of S-doped CN (S-CN) as an efficient, scalable, and stable photocatalyst with high photoactivity and selectivity for toluene oxidation to benzaldehyde and benzoic acid. We introduce a simple rational design of S-CN photocatalysts via tailored supramolecular assemblies,[36] containing bismuthiol as the S source.[39,40] The optimal photocatalyst (CN-CMBT$_1$) permits toluene oxidation to benzaldehyde, with a ≈100% conversion, demonstrating average benzaldehyde and benzoic acid yields of 72% ± 11% and 26% ± 14%, respectively. Prolonging the reaction time further produced benzoic acid as the sole product, highlighting the unique ability of CN-CMBT$_1$ to tune the toluene oxidation selectivity to either benzaldehyde or benzoic acid as a function of reaction time. Moreover, CN-CMBT$_1$ photocatalyst panels (i.e., 7.2 × 2.0 cm^2 films on glass) show high stability for up to one month in pure toluene batch reaction conditions, achieving an average reaction rate of 88.5 µmol m^{-2} h^{-1} with benzaldehyde as the major oxidation product.

2. Results and Discussion

2.1. Synthesis and Characterization of the Photocatalytic Materials

Sulfur-incorporated carbon nitride materials (CN-CMBT$_x$) were synthesized by adding different amounts (x designates the amount in mmol ranging from 0 to 2) of bismuthiol (2,5-dimercapto-1,3,4-thiadiazole; abbreviated as BT) as a sulfur source to 4 mmol of melamine (M) and dissolving them in water. This solution is mixed with another aqueous solution containing 4 mmol of cyanuric acid (C), as shown in **Figure 1a**.[36,40,41] After mixing the monomers for 1 h, a supramolecular CMBT$_x$ aggregate forms, and after polymerization at 550 °C for 4 h under N_2(g), the final photocatalyst powder (CN-CMBT$_x$) is obtained. Extensive characterization was performed on the CN-CMBT$_x$ series, with particular emphasis on the CN-CMBT$_1$ due to its high photocatalytic performance, as discussed later. The control CN photocatalyst, CN-CM (no S source), was also analyzed for comparison. The morphology of the prepared powders was studied by scanning electron microscopy (SEM), showing important structural changes depending on the relative amount of added bismuthiol.

The photocatalyst powder (Figure 1b) is altered by the incorporation of bismuthiol in the precursor, which leads to a porous, elongated rod-like morphology, as shown in Figure 1c for the CN-CMBT$_x$ product after thermal polymerization. Analysis of the specific surface area (S_A) shows an increase in S_A as a function of BT in the precursor—from 82.5 m^2 g^{-1} in the control CN-CM up to the highest value in CN-CMBT$_1$ (S_A = 144.9 m^2 g^{-1}), as a result of H_2S release during thermal polymerization.[6] After this optimum, a decrease in S_A is detected (Figure 1d). Fourier-transform infrared spectroscopy (FTIR) of CN-CMBT$_x$ materials (Figure S1a, Supporting Information) shows typical stretching modes of CN heterocycles from 1200 to 1600 cm^{-1}, the stretching mode of triazine units at 800 cm^{-1}, and stretching modes of N–H from 3000 to 3400 cm^{-1} due to free NH_x.[40,42]

The X-ray diffraction patterns (XRD) of CN-CMBT$_x$ materials are shown in Figure 1e. All the CN materials show two typical diffraction signals of polymeric carbon nitrides based on a heptazine repeating unit. The diffraction ca. 27.5° corresponds to the (002) plane, representing interlayer stacking of CN layers. Compared to the control, CN-CMBT$_x$ exhibits a shift of 0.4° toward a lower angle, indicating a larger average stacking distance between two CN planes. The in-plane (100) pattern of CN ≈2θ = 12.7° also shows a slight shift upon sulfur incorporation. Thus, XRD analysis supports the higher porosity detected by SEM images and nitrogen sorption experiments, without modification of the functional groups (i.e., FTIR spectra).[40,41]

X-ray photoelectron spectroscopy (XPS) analysis was used to determine the chemical state of the elements at the CN's surface (Figure 1f–g; Figure S1b–f, Supporting Information). The high-resolution C 1s spectrum of CN-CMBT$_1$ can be deconvoluted into four peaks centered at 284.9, 286.7, 288.1, and 288.9 eV, which correspond to C–C, C–S, C═N–C, and C–O bonds, respectively (Figure 1f).[41] Furthermore, the high-resolution N 1s spectrum (Figure S1c, Supporting Information) also displays four different binding energies at 398.7, 399.2, 400.1, and 401.1 eV, which are attributed to pyridinic N (C═N–C), tertiary N (N–(C)$_3$), primary N (from –NH_2 groups), and quaternary N, respectively.[43] The high-resolution S 2p spectrum is deconvoluted into different peaks at 164.5–165 and 167.7–168.7 eV, corresponding to C–S and C–SO_x (x = 2, 3, 4) sulfur oxide groups (Figure 1g).[44,45] The C 1s spectrum of control CN-CM material is deconvoluted into three different peaks at 284.9, 288.1, and 288.9 eV, which correspond to C–C, C═N–C, and C–O bonds, respectively (Figure S1d, Supporting Information).[41] As expected, CN-CM (the control sample) has no peaks in its S 2p spectrum (Figure S1e, Supporting Information) since there is no S in its structure. On the other hand, the N 1s spectrum of CN-CM (Figure S1f, Supporting Information) is similar to CN-CMBT$_1$ since sulfur does not bond with nitrogen in this system.

The optical properties of the CN-CMBT$_x$ materials were analyzed using diffuse reflectance ultraviolet–visible (UV–vis) spectroscopy. As shown in **Figure 2a**, the UV–vis spectra illustrate that the absorbance is enhanced into the visible region with an increasing amount of BT in the CN precursors. Moreover, the corresponding Tauc plots show a decrease in the estimated band gap of CN-CMBT$_x$ samples upon increasing x compared to CN-CM (Figure S2a, Supporting Information). The valence band (VB) positions were calculated using XPS, and exhibit a positive shift with increasing x, as illustrated in Figure S2b–f (Supporting Information). The VB positions (E_{VB}) and the optical bandgaps (E_g) allow the construction of CN-CMBT$_x$ energy band diagram on the normal hydrogen electrode (NHE) scale (Figure 2b). It demonstrates how the increasing incorporation of the third sulfur-containing monomer, BT, into the supramolecular assembly results in a consistent positive shift of the energy bands, effectively tuning the resulting CN-CMBT$_x$'s electronic structure and band gap.

Photoluminescence (PL) measurements of the CN-CMBT$_x$ samples show lower fluorescence intensity in comparison to the

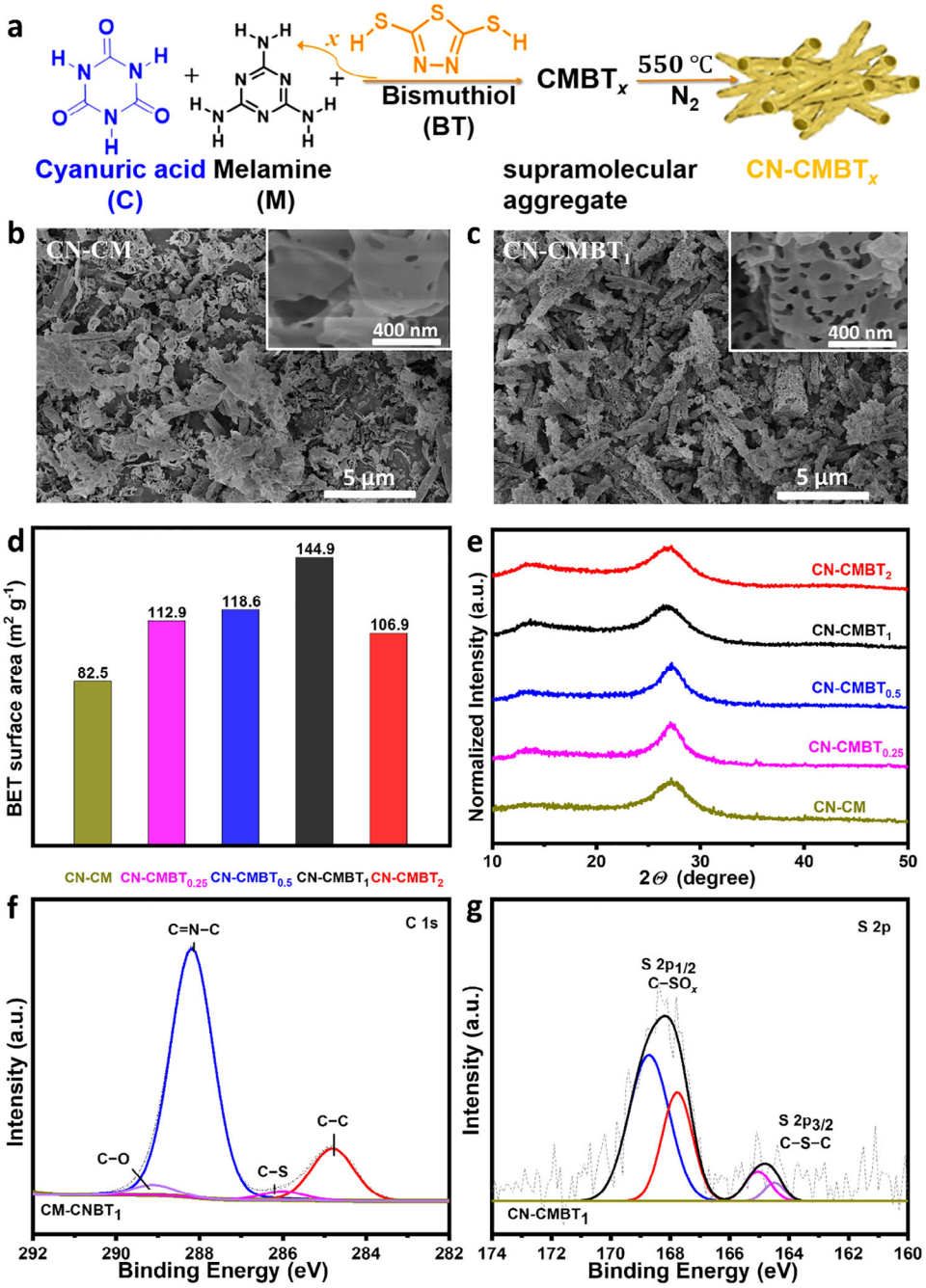

Figure 1. Characterization of CN-CMBT$_x$. a) Schematic of sulfur-doped polymeric carbon nitride synthesis via supramolecular preorganization. SEM images of (b) CN-CM, and (c)CN-CMBT$_1$. d) Estimated specific surface area (BET model). e) XRD patterns. f) C 1s, and (g) S 2p XPS spectra of CN-CMBT$_1$.

control CN-CM, implying a possible improved charge separation efficiency[41] as a result of introducing BT (Figure 2c).

Electron paramagnetic resonance (EPR) spectroscopy (Figure 2d) reveals that CN-CM exhibits a single *g*-factor of ≈2.003, which is attributed to unpaired electrons in the π-conjugated structure of tri-*s*-triazine units within the polymerized CN network.[23,46] However, the CN-CMBT$_1$ shows an additional *g*-factor at 2.004 (Figure 2d; Figure S3, Supporting Information), which we attribute to new surface paramagnetic centers near heteroatoms. These centers may result from sulfur doping, owing to the increased unpaired electron density compared to CN-CM.[46] Energy-dispersive X-ray spectroscopy (EDS) and X-ray photoelectron spectroscopy (XPS) analyses reveal a sulfur atomic content in the 0.1–1.4% range for CN-CMBT$_1$, as shown in Tables S1–S2 (Supporting Information), in line with previous reports showing that upon polymerization only

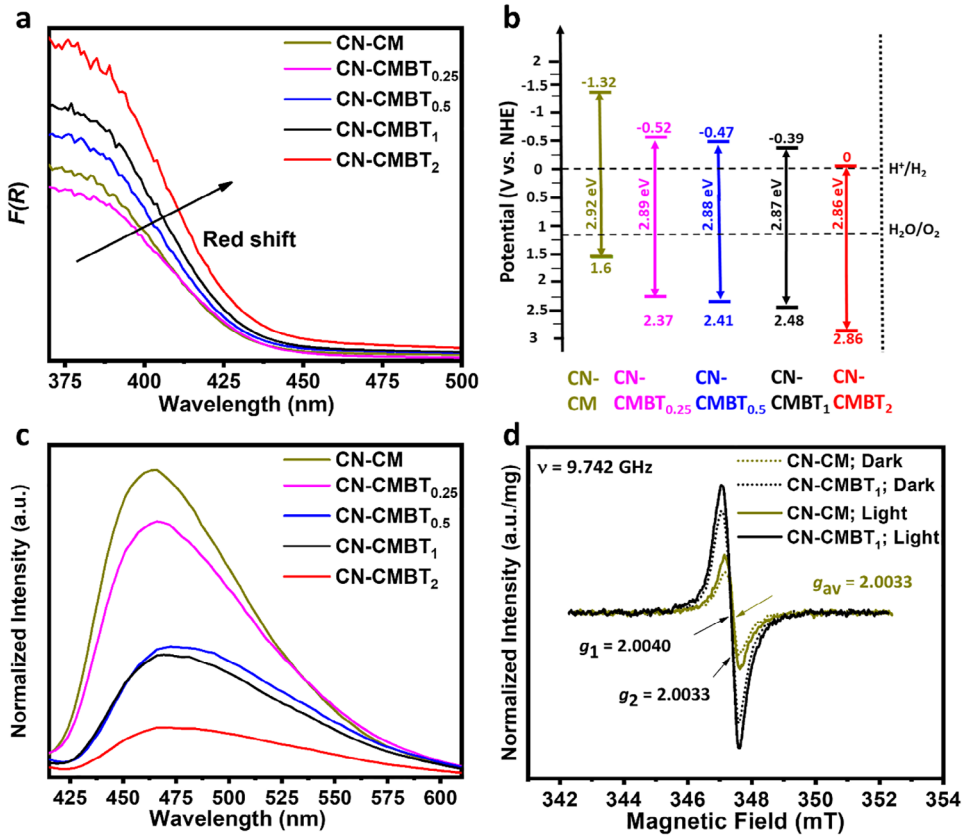

Figure 2. Optical characterization and band positions estimation of CN-CMBT$_x$. a) UV–vis diffuse reflectance spectra. b) Proposed energy band positions diagram. c) Photoluminescence emission spectra (excitation wavelength: λ_{ex} = 395 nm). d) EPR analysis of CN-CM and CN-CMBT$_1$ powders.

residual S remains in the CN structure.[40] Despite the very low remaining sulfur in the CN structure, it affects the S_A (as discussed earlier, with the highest value for CN-CMBT$_1$), and its influence is also detected by EPR (for CN-CMBT$_1$). When subjected to an irradiation (30 W white LED), the EPR signals for both CN-CM and CN-CMBT$_1$, increase in intensity, relative to a measured in the dark (complete versus dashed lines in Figure 2d, respectively), serving as an indication of the presence of photogenerated charges in the photocatalyst powders. The higher intensity of the EPR signal (normalized to the mass of the catalyst) may indicate improved charge generation or separation[47] in the CN-CMBT$_1$ photocatalyst relative to the CN-CM control.

2.2. Photocatalytic Toluene Oxidation

Photocatalytic experiments (constant 100 W white LED irradiation; constant temperature T = 25 °C) were performed using continuously stirred photocatalyst powders in a batch photoreactor containing the reaction medium, consisting of acetonitrile as the solvent and toluene as the reactant. All liquid products were analyzed using high-performance liquid chromatography (HPLC) and gas chromatography–mass spectrometry (GC–MS), quantified using the calibration curves (Figures S4–S5, Supporting Information) provided in the Supporting Information.

Typically, photooxidation of toluene can produce benzaldehyde (BzAl), benzyl alcohol (BnOH), and benzoic acid (BnCOOH), as shown in **Figure 3a**.[3,14,23] The S-CN photocatalysts enable higher BzAl yields than pristine CN after a 4 h reaction (Figure 3b). CN-CMBT$_1$ has the highest BzAl yield with ≈80% selectivity, almost 8 times higher than pristine CN-CM.

To validate the good activity and reproducibility of CN-CMBT$_1$ photocatalysts for toluene oxidation, we repeated the same experiment five times (Figure S6a–b, Supporting Information). The CN-CMBT$_1$ maintained an average toluene conversion of 99.8% ± 0% after 24 h (Figure 3c). The primary products were BzAl (an average yield of 72% ± 11%) and BnCOOH (an average yield of 26% ± 14%). The average sum of both BzAl and BnCOOH average yields were calculated to be ≈98.2% ± 3%, which is almost matching with the obtained average conversion of toluene (the slight difference might be due to an unknown product, which we couldn't detect). In contrast, the control CN-CM achieves a conversion of only 48.1% with 46.3% BzAl yield without detected BnCOOH. Prolonged 48 h reactions using CN-CMBT$_1$ reveal that BzAl is further oxidized to BnCOOH (Figure S6c, Supporting Information). After 24 h, the BzAl and BnCOOH yields are 79.9% and 20.1%, respectively, with close to 100% toluene conversion. Prolonging the reaction to 48 h shows a decrease in the BzAl yield to 0.9% with a simultaneous increase of BnCOOH yield to 73.4%.

A similar experiment was conducted using BzAl instead of toluene as the reactant to evaluate the ability of CN-CMBT$_1$ to

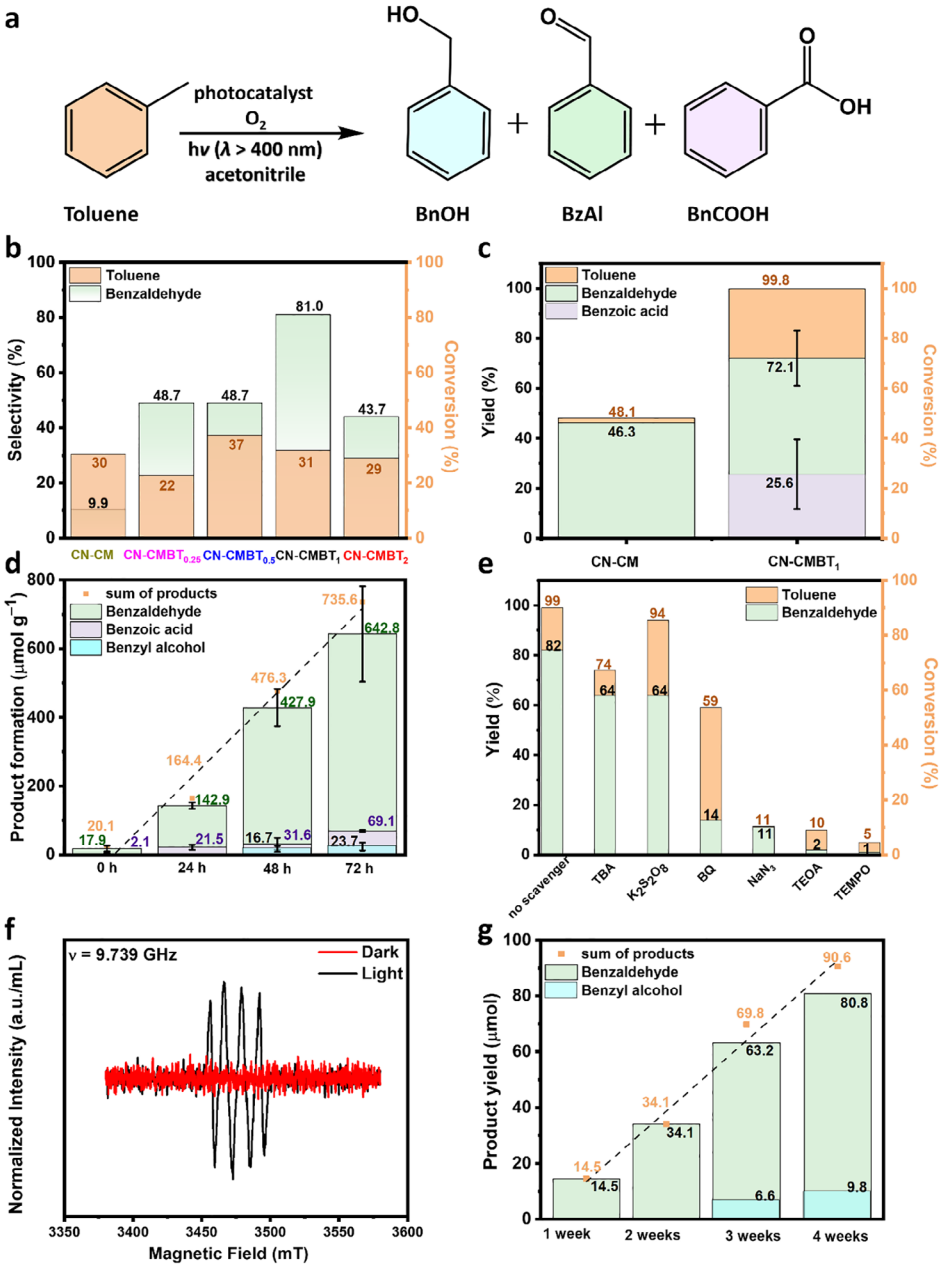

Figure 3. (a) General toluene photooxidation scheme with the three major possible products: benzyl alcohol, benzaldehyde, and benzoic acid. b) Toluene conversion (right *y*-axis) and benzaldehyde selectivity (left *y*-axis); conditions: 5 mg photocatalyst (continuously stirred), 0.01 mmol toluene, 3 mL acetonitrile, $t = 4$ h. c) Photocatalytic toluene oxidation performance of CN-CM and CN-CMBT$_1$ after 24 h (for CN-CMBT$_1$, the average reproducibility of five separate reactions is shown). d) Prolonged reaction study in 100% toluene; conditions: 10 mg CN-CMBT$_1$ (continuously stirred), 6 mL pure toluene (the average reproducibility of three separate reactions). e) A mechanistic study by adding 1.5 mmol of various scavengers. f) EPR toluene oxidation experiment in the presence of DMPO. g) Prolonged reaction using a photocatalyst panel; conditions: 7.2 × 2.0 cm^2 glass/CN-CMBT$_1$ in 120 mL pure toluene. In all experiments a constant temperature $T = 25$ °C and O_2 pressure were maintained.

produce BnCOOH selectively. As shown in Figure S6d (Supporting Information), the CN-CMBT$_1$ converts 99.7% of the BzAl to BnCOOH with a yield of 99.7%. In contrast, the CN-CM showed ≈66% BzAl conversion with only 49.4% BnCOOH yield. To further confirm the BzAl photooxidation route to BnCOOH, we have performed a control reaction without adding an S-CN photocatalyst, which showed only a ≈3% BzAl conversion with 2% BnCOOH yield even after 24 h illumination under an O_2 atmosphere, ruling out the self-oxidation, corroborating the ability of CN-CMBT$_1$ to produce BnCOOH (Figure S6d, Supporting Information). The other products remain unidentified and are not detected in HPLC or GC–MS analyses. The high photocatalytic performance of CN-CMBT$_1$ is attributed to the structural and photophysical properties modifications, mainly the band structure,

charge separation, and increased specific surface area compared to CN-CM.

Based on the above encouraging results, we performed a toluene photooxidation reaction without acetonitrile as a solvent since solvent-free toluene oxidation is more practically convenient for product separation and potentially more sustainable.[48,3,44,14] As illustrated in Figure 3d, the yields of BzAl and BnCOOH increased progressively over time, when the S-CN photocatalyst is dispersed in pure toluene and illuminated, consistent with earlier results obtained in acetonitrile. After 72 h, the reaction yielded 642.8 ± 139.0 μmol g^{-1} of BzAl, 69.1 ± 3.2 μmol g^{-1} of BnCOOH, and a lower amount of BnOH (23.7 ± 11.5 μmol g^{-1}). Fitting the total formed products as a function of time reveals a pseudo zero order reaction, with a (normalized to the mass of S-CN photocatalyst) rate constant of 9.9 ± 3.5 μmol g^{-1} h^{-1}. The observable zeroth order kinetics is expected from a reaction in pure toluene (i.e., excess reactant), where the first step in the mechanism ($C(sp^3)$−H activation in the toluene reactant) was reported as the rate-determining step.[3] These results emphasize the high catalytic efficiency of CN-$CMBT_1$ in promoting the photooxidation of toluene to BzAl and BnCOOH, even under solvent-free conditions. Moreover, it shows the comparability of the reported CN with the different catalysts in the selectivity of toluene photooxidation (Table S3, Supporting Information).

2.3. Mechanism Study

To corroborate a photooxidation mechanism over the catalyst, several control experiments were conducted: i) under Ar (i.e., O_2-free), ii) in the dark with a catalyst, and iii) under illumination without a catalyst. All resulted in low-to-negligible toluene conversion and BzAl yields, confirming the necessity of light, photocatalyst, and O_2 (Figure S6e, Supporting Information). To verify the possible mechanistic pathway and establish the responsible major reactive oxygen species (ROS) for toluene oxidation[3,23,30] over CN-$CMBT_1$, experiments in the presence of scavengers were performed. Here, *t*-butanol (TBA), potassium persulfate ($K_2S_2O_8$), *para*-benzoquinone (BQ), sodium azide (NaN_3), triethanolamine (TEOA), and *tetra*-methylpiperidine *N*-oxide (TEMPO) were used as •OH, electron, superoxide ($O_2^{\bullet-}$), singlet oxygen ($^1O_2$), hole, and all radical scavengers, respectively. As shown in Figure 3e, the presence of BQ, NaN_3, and TEOA results in a dramatic decrease in the yield of BzAl compared to the control experiment with no scavengers, which confirms the major role of $O_2^{\bullet-}$, $^1O_2$, and holes in toluene photooxidation. Moreover, the presence of TBA slightly decreases the BzAl yield, indicating a minor role of •OH radical. Finally, the addition of TEMPO completely suppresses toluene oxidation, demonstrating the pivotal role of radicals in this photocatalytic reaction.

EPR experiments mimicking the same condition of toluene oxidation in the presence of 1.5 mmol of 5,5-dimethyl-1-pyrroline *N*-oxide (DMPO) confirm the involvement of $O_2^{\bullet-}$ as the primary radical in the toluene oxidation reaction, formed when the photocatalyst is illuminated. The EPR spectrum (Figure 3f) shows the formation of $O_2^{\bullet-}$ or •OOH, as evidenced by the signals detected after 15 min of illumination. These signals intensified over time, indicating an increasing $O_2^{\bullet-}$ concentration. No EPR signals are observed after 15 min in the dark, emphasizing that light is essential for $O_2^{\bullet-}$ generation and, thereby, toluene oxidation. No additional radicals other than $O_2^{\bullet-}$ were detected despite continued illumination for 75 min (Figure S6f, Supporting Information). Similar EPR tests with BzAl instead of toluene confirmed the presence of $O_2^{\bullet-}$, supporting the role of $O_2^{\bullet-}$ for BzAl oxidation to BnCOOH (Figure S7a,b, Supporting Information).

To confirm the participation of $^1O_2$ in the toluene photooxidation reaction under our experimental conditions, a series of experiments were conducted (Figure S8, Supporting Information). The $^1O_2$ can oxidize 1,5-dihydroxynaphthalene (1,5-DHN) to produce 5-hydroxynaphthalene-1,4-dione (juglone).[49,50] As shown in the UV–vis spectra (Figure S8a, Supporting Information), the concentration of 1,5-DHN decreased over time alongside juglone concentration increase, indicating the ability of CN-$CMBT_1$ to generate $^1O_2$. An additional experiment in the presence of toluene also showed a decrease in 1,5-DHN concentration over time with increasing juglone concentration using CN-$CMBT_1$ (Figure S8c, Supporting Information), confirming the role of $^1O_2$ during toluene oxidation. A similar reaction conducted by using BzAl instead of toluene also confirmed the presence of $^1O_2$, further supporting the role of $^1O_2$ in BzAl oxidation to BnCOOH (Figure S8e, Supporting Information).

Based on our results, we propose a possible mechanism for the toluene photooxidation reaction (Figure S9, Supporting Information). Under illumination, the excited CN-$CMBT_1$ activates surface-adsorbed O_2 to $O_2^{\bullet-}$ (one-electron reduction) or to $^1O_2$ by energy transfer. In parallel, photogenerated holes from the CN-$CMBT_1$ oxidize toluene to benzyl radicals by proton abstraction. The benzyl radicals can react with a $O_2\cdot^-$ and a proton or alternatively, $^1O_2$ directly reacts with toluene to produce benzyl hydroperoxide. These benzyl hydroperoxide intermediates dehydrate to BzAl. At longer reaction times, a similar oxidative mechanism occurs with BzAl, leading to its subsequent conversion into BnCOOH.[3,30,51,52]

2.4. Recyclability

Five cycles of recyclability experiments were performed, confirming the good stability of the CN-$CMBT_1$ photocatalyst (Figure S10a, Supporting Information). The CN-$CMBT_1$ retained ≈64% of its initial activity after the fifth cycle. Post-operational analysis (FTIR, XRD, and UV–vis spectroscopy) shows similar structural and photophysical properties as a fresh sample while the morphology changed according to SEM images (Figure S10b–f, Supporting Information). The decrease in the photocatalytic activity might result from the unavoidable gradual catalyst mass loss during washing of the catalyst between consecutive cycles and the morphological changes observed in the SEM, phenomena that can be mitigated using photocatalyst panels instead of continuously-stirred powdered catalysts.

2.5. Batch Toluene Photooxidation Over CN-$CMBT_1$ Panels

Based on the encouraging photocatalytic results with CN-$CMBT_1$ powder for aerobic toluene oxidation, this reaction was also performed as a proof-of-concept over binder-free CN panels. CN-$CMBT_1$ panels on glass and fluorine-doped tin oxide-coated glass

(FTO) substrates were successfully prepared by adapting our previous reports,[39,40,42] as shown in Figure S11 (Supporting Information).

The photocatalytic experiments were performed in a batch configuration (Figure S12, Supporting Information), where the obtained 1.2 × 1.2 cm^2 substrate/CN-$CMBT_1$ was placed in 5 mL of pure toluene (Figure S12a, Supporting Information). Up to 11 days of photocatalysis over glass/CN-$CMBT_1$ panels (Figure S13a, Supporting Information), results in 7.48 µmol of BzAl with trace amounts of BnOH (0.9 µmol) and BnCOOH (0.001), respectively. An FTO/CN-$CMBT_1$ panel under similar experimental conditions (Figure S13b, Supporting Information) yields 6.04 µmol BzAl and 0.90 µmol BnOH without any detected BnCOOH. Unlike CN-$CMBT_1$ powder, the CN-$CMBT_1$ panels resulted in the formation of BnOH as a minor product without any formation of BnCOOH, which might result from a side reaction between two formed benzyl hydroperoxide intermediates ($C_6H_5CH_2OOH$) to yield BnOH and BzAl. A plausible mechanism and relevant discussion are given in the Supporting Information (Figure S13c, Supporting Information). After 11 days of toluene oxidation, the glass/CN-$CMBT_1$ and FTO/CN-$CMBT_1$ samples were characterized using FTIR, XRD, and UV–vis spectroscopy (Figure S14, Supporting Information), confirming that the CN remains almost unaltered.

With these positive results using small CN panels, we scaled up this batch reaction with 7.2 × 2.0 cm^2 size of glass/CN-$CMBT_1$ panel for one month (Figure S12b, Supporting Information). After four weeks, the glass/CN-$CMBT_1$ panel produced ≈80.8 µmol of BzAl and 9.8 µmol of BnOH without any detected BnCOOH with an average product formation rate of ≈88.5 µmol m^{-2} h^{-1} (Figure S15, Supporting Information).

3. Conclusion

This work introduced a highly active and stable CN photocatalyst for selective aerobic toluene oxidation to benzaldehyde and benzoic acid. To do so, we developed a simple and effective method for synthesizing sulfur-doped CN with improved optical absorbance, tuned energy band positions, high specific surface area, and unique structural properties using a sulfur-containing supramolecular assembly as a precursor comprising three monomers: cyanuric acid, melamine, and bismuthiol. The optimal photocatalyst (CN-$CMBT_1$) exhibits high photocatalytic activity and selectivity, with 72% ± 11% benzaldehyde and 26% ± 14% benzoic acid after 24 h. Prolonging the reaction time until 48 h further produced benzoic acid as the main product (73.4%) with benzaldehyde at trace amounts (0.9%), highlighting the unique ability of CN-$CMBT_1$ to tune the toluene oxidation selectivity to either benzaldehyde or benzoic acid as a function of reaction time. Furthermore, we successfully grew CN-$CMBT_1$ layers on glass substrates, using them as photocatalytic binder-free panels, demonstrating the proof-of-concept photooxidation of toluene using photocatalytic solar panels in batch mode for one month. This study provides a facile design of functional CN-based powder and panel photocatalysts for the highly challenging C(sp^3)–H activation reactions and showcases their practical application in photoreactors.

4. Experimental Methods

Detailed experimental procedures (materials, characterization, photocatalytic panel synthesis, product quantification, and calibration curves) are given in the Supporting Information.

Synthesis of CN Precursors (CM and $CMBT_x$): The sulfur-incorporated polymeric carbon nitride materials were synthesized by using bismuthiol as the sulfur source.[39,40] Two separate 50 mL centrifuge tubes, filled with 35 mL DI water were used to prepare aqueous solutions. To the first 4 mmol melamine with varying amounts (x = 0, 0.25, 0.5, 1, or 2 mmol) of bismuthiol was added (x = 0, being the control, with no bismuthiol). To the second tube 4 mmol cyanuric acid was added. Each tube was shaken overnight (≈12 h) using an automatic shaker at 500 rpm, separately. The content of both two tubes was mixed for 1 h, to form a supramolecular complex from an aqueous phase. The resulting supramolecular assemblies (CM as a control assembly without BT, and $CMBT_x$) were isolated by filtration and washed with deionized (DI) water. The resulting powders were dried for 12 h at 70 °C in a vacuum oven, and these powders were used for the next step.

Synthesis of Photocatalyst Powders (CN-CM and CN-$CMBT_x$): The obtained $CMBT_x$ and CM powders were placed in a ceramic crucible and covered with a lid. Subsequently, the crucible was placed in a muffle furnace and a heating procedure commenced under a constant nitrogen flow. First, the temperature increased from room temperature to 80 °C for 1 h ($dT/dt \approx 1$ °C min^{-1}), followed by heating to the target temperature of 550 °C with a constant heating ramp ($dT/dt \approx 2.5$ °C min^{-1}). Upon reaching the target temperature, the furnace was maintained at 550 °C for 4 h before natural cooling back to room temperature. The products are labeled as CN-CM or CN-$CMBT_x$ and used as photocatalysts.

Photocatalytic Toluene Oxidation: The photocatalytic activity of the heterogeneous photocatalysts was evaluated for toluene photooxidation to benzaldehyde and benzoic acid under the illumination of a white LED (100 W, white light, $\lambda > 400$ nm).[42] Briefly, 5 mg of the catalyst was dispersed in 3 mL of acetonitrile, and 0.01 mmol of toluene was added to the suspension.[23] For solvent-free toluene photooxidation experiments using powder catalyst, 10 mg of the photocatalyst was dispersed in 6 mL of pure toluene. O_2 gas was bubbled for 5 min before sealing the reaction tube with a rubber septum. A constant O_2 pressure was maintained using an O_2-filled balloon during the reaction. The reaction mixture was continuously-stirred at 600 rpm under illumination for a fixed time. A constant reaction temperature (T = 25 °C) was maintained using a double-wall glass jacker connected to a circulating water bath.

For batch reactions using CN panels, the CN panel directly placed in pure toluene (7.2 × 2.0 cm^2 glass/CN-$CMBT_1$ panel was placed in 120 mL of pure toluene or 1.2 × 1.2 cm^2 glass or FTO/CN-$CMBT_1$ panel was placed in 5 mL of pure toluene). The image of the reaction setup is provided in supporting information (Figure S12, Supporting Information). After the reaction, the liquid products were identified using HPLC using a C-18 column and a diode array detector (DAD). The liquid products were also confirmed using GC–MS.

Supporting Information

Supporting Information is available from the Wiley Online Library or from the author.

Acknowledgements

This project has received funding from the European Research Council (ERC) under the European Union's Horizon 2020 Research and Innovation Program (Grant Agreement No. 849068). This work was partially supported by the Israel Science Foundation, Grant No. 601/21. B.A. acknowledges the Yad Hanadiv Fellowship (Natural Sciences Scholarships for Arab M.Sc. Students in STEM Fields), and Dr. Nitzan Maman from the Ilse-Katz Institute for Nanoscale Science and Technology for some SEM measurements.

Conflict of Interest

The authors declare no conflict of interest.

Data Availability Statement

The data that support the findings of this study are available from the corresponding author upon reasonable request.

Keywords

bismuthiol, carbon nitride, photocatalysis, photooxidation, toluene oxidation

Received: January 29, 2025
Revised: March 12, 2025
Published online: March 27, 2025

[1] Z. J. Bai, S. Tian, T. Q. Zeng, L. Chen, B. H. Wang, B. Hu, X. Wang, W. Zhou, J. B. Pan, S. Shen, J. K. Guo, T. L. Xie, Y. J. Li, C. T. Au, S. F. Yin, *ACS Catal.* **2022**, *12*, 15157.
[2] X. Q. Yao, X. J. Hou, G. S. Wu, Y. Y. Xu, H. W. Xiang, H. Jiao, Y. W. Li, *J. Phys. Chem. A* **2002**, *106*, 7184.
[3] H. Wang, C. Cao, D. Li, Y. Ge, R. Chen, R. Song, W. Gao, X. Wang, X. Deng, H. Zhang, B. Ye, Z. Li, C. Li, *J. Am. Chem. Soc.* **2023**, *145*, 16852.
[4] X. Zhan, C. Ding, Q. H. Zhao, Y. Fang, *Opt. Mater.* **2024**, *155*, 115860.
[5] H. H. El-Maghrabi, S. A. Younis, H. R. Ali, A. A. Nada, *J. Environ. Chem. Eng.* **2023**, *11*, 109477.
[6] W. Partenheimer, *Catal. Today* **1995**, *23*, 69.
[7] C. Subrahmanyam, B. Louis, F. Rainone, B. Viswanathan, A. Renken, T. K. Varadarajan, *Catal. Commun.* **2002**, *3*, 45.
[8] A. Martin, U. Bentrup, A. Brückner, B. Lücke, *Catal. Lett.* **1999**, *59*, 61.
[9] F. Konietzni, H. W. Zanthoff, W. F. Maier, *J. Catal.* **1999**, *188*, 154.
[10] A. Martin, U. Bentrup, G.-U. Wolf, *Appl. Catal.* **2002**, *227*, 131.
[11] Y. Ishii, S. Sakaguchi, T. Iwahama, *Adv. Synth. Catal.* **2001**, *343*, 393.
[12] T. Punniyamurthy, S. Velusamy, J. Iqbal, *Chem. Rev.* **2005**, *105*, 2329.
[13] F. Wang, J. Xu, X. Li, J. Gao, L. Zhou, R. Ohnishi, *Adv. Synth. Catal.* **2005**, *347*, 1987.
[14] X. Cao, Z. Chen, R. Lin, W. C. Cheong, S. Liu, J. Zhang, Q. Peng, C. Chen, T. Han, X. Tong, Y. Wang, R. Shen, W. Zhu, D. Wang, Y. Li, *Nat. Catal.* **2018**, *1*, 704.
[15] S. Okunaka, H. Tokudome, Y. Hitomi, *J. Catal.* **2020**, *391*, 480.
[16] B. Yuan, B. Zhang, Z. Wang, S. Lu, J. Li, Y. Liu, C. Li, *Chin. J. Catal.* **2017**, *38*, 440.
[17] L. N. Song, L. Chen, J. He, P. Chen, H. K. Zeng, C. T. Au, S. F. Yin, *Chem. Commun.* **2017**, *53*, 6480.
[18] L. N. Song, F. Ding, Y. K. Yang, D. Ding, L. Chen, C. T. Au, S. F. Yin, *ACS Sustain. Chem. Eng.* **2018**, *6*, 17044.
[19] K. Su, H. Liu, B. Zeng, Z. Zhang, N. Luo, Z. Huang, Z. Gao, F. Wang, *ACS Catal.* **2020**, *10*, 1324.
[20] Y. Zhang, N. Zhang, Z. R. Tang, Y. J. Xu, *Chem. Sci.* **2012**, *3*, 2812.
[21] F. Liu, C. X. Xiao, L. H. Meng, L. Chen, Q. Zhang, J. Bin Liu, S. Shen, J. K. Guo, C. T. Au, S. F. Yin, *ACS Sustain. Chem. Eng.* **2020**, *8*, 1302.
[22] B. Rawat, V. R. Battula, P. K. Nayak, D. Ghosh, K. Kailasam, *ACS Appl. Mater. Interfaces* **2023**, *15*, 53604.
[23] R. Ghalta, R. Srivastava, *Catal. Sci. Technol.* **2023**, *13*, 1541.
[24] L. Jing, H. Wang, Z. Li, P. Li, Q. Gao, J. Hu, *RCM.* **2024**, 100076.
[25] B. Lei, J. Sheng, F. Zhong, C. Du, Y. He, J. Li, F. Dong, *J. Catal.* **2024**, *429*, 115270.
[26] Z. J. Bai, Y. Mao, B. H. Wang, L. Chen, S. Tian, B. Hu, Y. J. Li, C. T. Au, S. F. Yin, *Nano. Res.* **2023**, *16*, 6104.
[27] J. Song, C. Zhang, H. Zhang, D. Dai, Q. Zhang, Z. Wang, Z. Zheng, Y. Liu, H. Cheng, Y. Dai, B. Huang, P. Wang, *J. Chem. Eng.* **2023**, *453*, 139748.
[28] X. Li, H. Mai, N. Cox, J. Lu, X. Wen, D. Chen, R. A. Caruso, *Chem. Mater.* **2023**, *35*, 3105.
[29] H. H. Zhang, Z. C. Zhou, Y. J. Dong, L. Zhang, H. Y. Chen, D. Bin Kuang, *Sol. RRL* **2021**, *5*, 2100559.
[30] S. Li, N. Huber, W. Huang, W. Wei, K. Landfester, C. T. J. Ferguson, Y. Zhao, K. A. I. Zhang, *Angew. Chem., Int. Ed.* **2024**, *63*, 202400101.
[31] S. Kumar, B. Bayarkhuu, H. Ahn, H. Cho, J. Byun, *Nano Trends* **2023**, *4*, 100023.
[32] Y. Fan, Y. Luo, X. Luo, X. L. Ni, *Green Chem.* **2024**, *26*, 12076.
[33] S. C. Yu, X. Li, L. Cheng, L. Liu, *Chem. - Eur. J.* **2024**, *30*, 202400668.
[34] J. Zhu, P. Xiao, H. Li, S. A. C. Carabineiro, *ACS Appl. Mater. Interfaces* **2014**, *6*, 16449.
[35] V. W. hei Lau, B. V. Lotsch, *Adv. Energy. Mater.* **2022**, *12*, 2101078.
[36] J. Barrio, M. Shalom, *ChemCatChem* **2018**, *10*, 5573.
[37] J. Barrio, M. Volokh, M. Shalom, *J. Mater. Chem. A* **2020**, *8*, 11075.
[38] L. Jiang, X. Yuan, Y. Pan, J. Liang, G. Zeng, Z. Wu, H. Wang, *Appl. Catal. B* **2017**, *217*, 388.
[39] N. Karjule, J. Barrio, L. Xing, M. Volokh, M. Shalom, *Nano. Lett.* **2020**, *20*, 4618.
[40] N. Karjule, J. Barrio, A. Tashakory, M. Shalom, *Sol. RRL* **2020**, *4*, 2000017.
[41] S. Dolai, J. Barrio, G. Peng, A. Grafmüller, M. Shalom, *Nanoscale* **2019**, *11*, 5564.
[42] V. R. Battula, G. Mark, A. Tashakory, S. Mondal, M. Volokh, M. Shalom, *ACS. Catal.* **2024**, *14*, 11666.
[43] S. Mondal, G. Mark, L. Abisdris, J. Li, T. Shmila, J. Tzadikov, M. Volokh, L. Xing, M. Shalom, *Mater. Horiz.* **2023**, *10*, 1363.
[44] H. Wang, Y. Bian, J. Hu, L. Dai, *Appl. Catal. B* **2018**, *238*, 592.
[45] Q. Xu, P. Pu, J. Zhao, C. Dong, C. Gao, Y. Chen, J. Chen, Y. Liu, H. Zhou, *J. Mater. Chem. A.* **2015**, *3*, 542.
[46] D. Dvoranová, Z. Barbieriková, M. Mazúr, E. I. García-López, G. Marcì, K. Lušpai, V. Brezová, *J. Photochem. Photobiol. A: Chem.* **2019**, *375*, 100.
[47] Y. Guo, T. Chen, Q. Liu, Z. Zhang, X. Fang, *J. Phys. Chem. C* **2016**, *120*, 25328.
[48] R. Yuan, S. Fan, H. Zhou, Z. Ding, S. Lin, Z. Li, Z. Zhang, C. Xu, L. Wu, X. Wang, X. Fu, *Angew. Chem., Int. Ed.* **2013**, *52*, 1035.
[49] J. Sun, J. Zhao, H. Guo, W. Wu, *Chem. Commun.* **2012**, *48*, 4169.
[50] E. E. Coyle, K. Joyce, K. Nolan, M. Oelgemöller, *Green Chem.* **2010**, *12*, 1544.
[51] J. He, L. Chen, D. Ding, Y. K. Yang, C. T. Au, S. F. Yin, *Appl. Catal. B* **2018**, *233*, 243.
[52] H. M. Lapa, L. M. D. R. S. Martins, *ACS Omega* **2024**, *9*, 26780.

